


Article

Research on Three-Dimensional Scanning Path Planning of Casing Parts Based on Industrial Robot

Jing Li ¹, Minghai Wang ^{2,*}, Ligang Qu ^{1,*} and Guangming Lv ³ 

¹ Aviation Manufacturing Technology Digital Defense Key Discipline Laboratory, Shenyang Aerospace University, Shenyang 110136, China; 20133362@sau.edu.cn

² School of Mechanical and Electrical Engineering, Shenyang Aerospace University, Shenyang 110136, China

³ School of Artificial Intelligence, Shenyang Aerospace University, Shenyang 110136, China; lv0527@163.com

* Correspondence: 19951876@sau.edu.cn (M.W.); 20062895@sau.edu.cn (L.Q.)

Featured Application: This paper analyzes the automatic scanning path planning method and the scanning quality influence rule for casing parts.

Abstract: According to the requirements for the rapid scanning and measurement of the geometric shape during the process of chemical milling of an aviation engine casing, the scanning path of the casing is planned and studied. This paper introduces the principle and method of the tracking scanner and automatic measuring system and analyzes the scanning area range, approach distance, and wide angle of the field. The casing process is modeled by applying part of the machine, obtaining a series of scanning path point and synthesizing the scanning trajectory. On this basis, the entire scanning process is divided into two alternating actions: scanning measurement and posture adjustment, and the mathematical model of the annular scanning path on the outer surface of the casing part is obtained. Adjusting the scan height was used to solve the repeated scan area problem, and the results show that the adjustment method effectively shortened the scan path's length and time. The simulation method verifies the planned finite ring-scanning path, which verifies the correctness and feasibility of the mathematical model. Through the automatic scanning reconstruction process test, the reconstruction rate of the ring scanning trajectory reaches 85%, which is 80% higher than the manual detection efficiency.



Citation: Li, J.; Wang, M.; Qu, L.; Lv, G. Research on Three-Dimensional Scanning Path Planning of Casing Parts Based on Industrial Robot. *Appl. Sci.* **2023**, *13*, 6162. <https://doi.org/10.3390/app13106162>

Academic Editors: Jin Guo, Wei Su and Wendong Xiao

Received: 5 April 2023
Revised: 24 April 2023
Accepted: 25 April 2023
Published: 17 May 2023



Copyright: © 2023 by the authors. Licensee MDPI, Basel, Switzerland. This article is an open access article distributed under the terms and conditions of the Creative Commons Attribution (CC BY) license (<https://creativecommons.org/licenses/by/4.0/>).

Keywords: casing; tracking scanning; scanning path planning; reconstruction rate

1. Introduction

With the continuous development of aero-engine manufacturing technology, under the premise of ensuring the high stability of aero-engines [1], the lightweight design and manufacture of aero-engine casings has become one of the most critical and effective technical means to improve the thrust-weight ratio of aero-engines. The casing is the basic skeleton of an aviation engine, comprising not only the central parts but also the main bearing parts of an aviation engine. The engine casing is a critical component of an aviation engine. Under the harsh conditions of high temperature and high pressure for a long time, it bears the high-temperature load and thrust load of the combustion chamber, and its manufacturing precision and performance requirements are incredibly high.

At present, the lightweight problem of aviation engine casing parts is solved mainly by chemical milling after traditional metal cutting [2]. Chemical milling removes the excess metal on the surface of the features, forming reinforcement and structural convex platform characteristics, reducing the weight of the self-structure without affecting the stress state of the casing elements. The chemically milled casing has characteristics of a thin wall, complex reinforced reinforcement structure, high precision, and weak rigid conical shell parts [3]. In the process of chemically milling the casing parts, it is necessary to measure the

casing many times during the chemical milling, to evaluate the machining accuracy of the casing parts and the effectiveness of the chemical milling process. The high concentration of acid corrosion liquid remaining on the surface of the pieces will also constantly corrode the parts during the measurement process [4], thus influencing wall thickness. Currently, this enterprise still uses the traditional ultrasonic thickness measurement method to measure the thickness of the critical position of the casing. In addition to the harsh operating environment, there is low detection efficiency and poor repetition accuracy in the results. The accurate measurement for the chemical milling process has become one of the greatest technological limitations in optimizing the chemical milling process and evaluating its lightweight-forming quality.

The surface shape of significant components is complex, and the manufacturing technology is complicated, so the morphology and size measurement has become the bottleneck that restricts the development and technological advancement of large equipment. Under field conditions, measuring the complex surface of significant components must meet the requirements for large scale, high point-cloud density, high precision, and high efficiency. Given the importance of the precision measurement of complex surfaces during the manufacturing of significant components in large equipment, the integrated automatic measurement method applicable to the industrial area has been studied [5]. Realizing the size of complex components requires both measurement accuracy and efficiency. The research background is described in Figure 1.

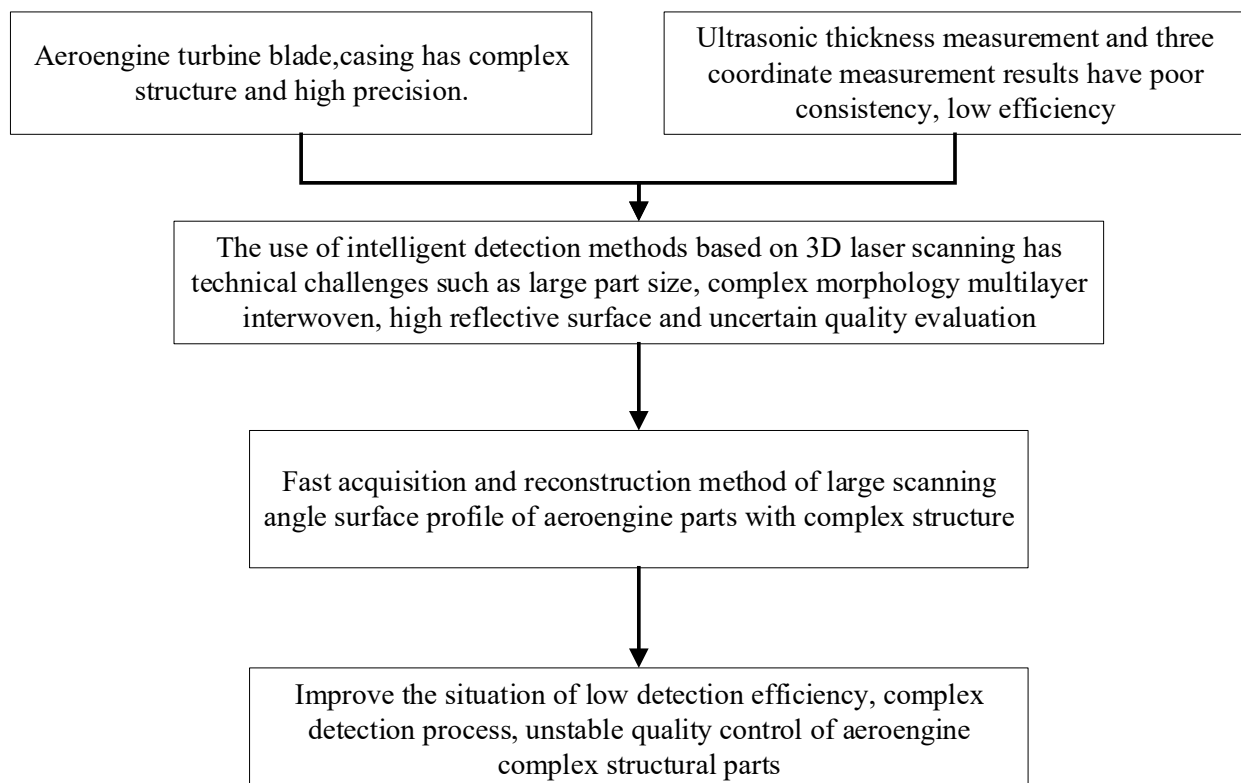


Figure 1. Research background for the key components of aero-engines.

As early as the 1980s, Germany began studying 3-D measurement technology in surface-structured light. In 1985, Dr. Breckmann introduced phase shift interferometry to three-dimensional morphology measurement, establishing a new three-dimensional morphology measurement technology: the phase-measurement contour technique (PMP) [6,7]. Additionally, Dr. Steinbichler and Professor Reinhold Ritter at Germany's Braunschweig Technical University introduced the Steinbichler GmbH COMET 5-3D measurement system [8,9] and the GOM GmbH Atos structural light 3-D measurement system [10]. In China,

Tsinghua University, Beijing University of Aeronautics and Astronautics, Shanghai Jiao Tong University, Xi'an Jiaotong University, Sichuan University, Huazhong University of Science and Technology, Tianjin University, and many other universities have also conducted systematic research on the stripe projection technology. At the same time, some commercial measurement systems, such as those produced by the Beijing Tianyuan 3D Technology Co., Ltd. (Beijing, China); Shanghai Shuzao Technology Co., Ltd. (Shanghai, China); Hangzhou Xianlin 3D Technology Co., Ltd. (Hangzhou, China); and Beijing Bowei Hengxin Technology Development Co., Ltd. (Beijing, China), etc., also launched 3-D measurement systems [11] based on stripe projection technology.

In industrial manufacturing, low measurement efficiency will delay the product's production cycle, and the measurement environment needs to maintain a relatively stable state throughout the product's production cycle; therefore, efficiency in the measurement process is needed to achieve automatic measurement. For the measurement of large, complex curved-surface components, the stripe projection sensors are required to measure the measured object in multiple poses, to realize the all-around coverage of the measured area of significant components. The high-precision fringe projection sensor needs to project multiple fringe images and keep the measured object stationary during the measurement process [12,13]. In addition, when measuring the global control points with the splicing camera based on close-up photogrammetry, it is also necessary to increase the number of poses to capture the global control points on the measured component to ensure accuracy [14]. The traditional close-view photogrammetry systems require manual operation, and the system is complex. Due to the advantages of high automation, high flexibility, and high efficiency of industrial robots, industrial robots were introduced into the measurement system. The fringe projection sensor and the stitching camera based on close-range photogrammetry are installed at the end of the robot through adapters to achieve automatic measurement within the range of motion [15]. Many researchers have optimized the scanning trajectory according to the parameters of the scanning system itself to obtain better scanning results and scanning efficiency. Generally, the scanning path can be generated by determining the point sequence of the scanning direction with the normal surface vector of the CAD model of the known part [16]. Nguyen [17] proposed a new path planning method that used a conformal map to stretch a 2D surface onto a 3D plane to control the overlap between two adjacent scanning paths. However, this method may cause a sudden change in the direction of the scanner between the two paths. Njaastad et al. [18] combined industrial robots with high-precision 3D cameras and laser distance sensors to form an automated scanning system to measure ship propeller blades. According to the shooting range of the 3D camera and the optimal proximity distance of the laser sensor, the scanning trajectory of the highly inclined ship propeller blade was planned with a resolution of 0.1 mm.

The above research shows that automatic 3D laser scanning is one of the key technologies to improve scanning efficiency and accuracy, and trajectory planning also plays an important role in automated laser-scanning systems. Aiming at the requirement of rapid thickness measurement in the chemical milling of casing parts, in this paper, a general scanning and measuring system composed of a six degrees of freedom industrial robot and tracking 3D scanner was designed. Its core part includes a six degrees of space parallel industrial robot and a three-dimensional tracking scanning system. The specific measurement process is as follows: (1) the three-dimensional point cloud data of the casing were obtained by automatically scanning the casing parts in the working area of the tracker through the six degrees of freedom industrial robot clamping the spherical scanning head; (2) the contoured fitting and post-processing of the point cloud data were carried out to realize the three-dimensional reconstruction of the measured workpiece; (3) the thickness measurement and analysis of the measured position were carried out in the Polyworks measurement software. For complex large-scale structural parts, it is time-consuming to plan the scanning path by manual teaching programming, and the spherical scanning head is easy to collide with the measured part. The accuracy of the scanning path also directly

affects the scanning efficiency and the reconstruction rate of the measured parts. Therefore, the planning of the scanning path is particularly important for popularizing automated 3D scanning systems in the measurement of large structural parts [19].

In this paper, the constraints such as scanning area range, proximity distance and scene width angle of the tracking 3D scanner are analyzed. Combined with the geometric structure characteristics of the casing parts, the mathematical model of the annular scanning path was established by using the mathematical discretization modeling method. The change rules of scanning stroke, robot attitude transformation times and scanning time under circular scanning path were analyzed. The Robot Studio software platform was used to simulate the automatic scanning trajectory, which verifies that the scanning trajectory meets the constraints. The influence of the scanning path on the scanning reconstruction rate was analyzed by scanning experimental results.

2. Automated Tracking Type 3D Scanning Measurement System

2.1. System Composition

In the manufacturing process of aeroengine large parts, it is necessary to quickly measure the geometric dimensions of the part to guide the manufacturing process and evaluate the processing quality. This paper designed an automatic tracking 3D scanning-measurement system with a laser 3D scanner and industrial robot as the core, which mainly includes a 3D scanning data acquisition subsystem (3D scanning head, laser positioning tracking instrument), motion control subsystem (industrial robot, safety protection), turntable support subsystem and software system (automatic scanning and detection software, system automatic control software), as shown in Figure 2. The motion control subsystem includes a six degrees of freedom industrial robot (called a scanning robot), which can flexibly scan the 3-D scanning head in the trapezoidal working space of the laser positioning tracker to realize the automatic acquisition of the point cloud of the casing engine. The turntable support subsystem is a six degrees of freedom parallel-motion platform, which can fix the measured workpiece in the measurement space of the laser positioning tracker, to realize the scanning measurement of multiple poses of the large aviation components.



Figure 2. Automatic tracking type 3D scanning measurement system.

The I/O module software system was developed to connect the scanning robot to the laser scanner through the I/O signal communication. The communication structure is shown in Figure 3. The I/O control signal was written into the robot scanning trajectory program, and the signal received/sent by the I/O module controls the three-dimensional scanning probe, laser positioning tracker and safety protection accessories for automatic scanning operations to complete the acquisition of the point cloud data of the measured workpiece.

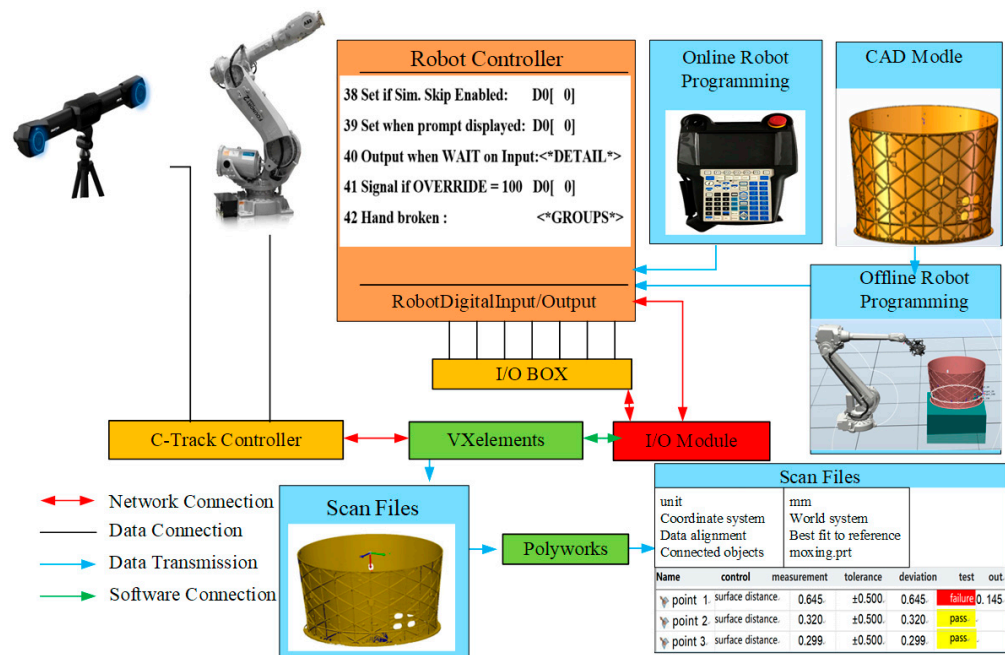


Figure 3. System communication structure.

The operation process of the automatic tracking-type 3D scanning measurement system to collect the point cloud data and measurement of casing parts: (1) the laser scanner, optical tracker, scanning robot and six degrees of freedom motion platform were calibrated in advance; (2) the measured casing was placed on a six degrees of freedom parallel motion platform, and the platform pose was adjusted to expose the inner and outer surfaces of the casing to the binocular camera of the laser location tracker as much as possible; (3) the laser scanner parameters were configured according to the material and reflectivity of the measured workpiece, and the scanning template was established; (4) the scanning path *.TB program of the scanning robot was established by teaching pendant or off-line programming method; (5) start the automatic control system, invocation of the scanning template and the scanning path *.TB program to scan the measured workpiece area by area to obtain its point cloud data; (6) the point cloud data of the workpiece were post-processed and imported into the measurement software. The casing wall thickness was measured according to the pre-established measurement program, and the measurement report was generated.

2.2. System Scanning Principle and Technical Parameters

The automatic tracking 3D scanning measurement system takes the optical tracker and the three-dimensional scanner as the core components, and its scanning principle is shown in Figure 4. The coordinate system of the three-dimensional scanning probe is O_B , the laser generator emits a laser line projected onto the scanned object, and the laser changes with the shape of the measured object. The coordinate system of the binocular camera of the 3D scanner is O_B , and the camera can obtain the three-dimensional coordinates of the laser projected onto the scanned object. The point P is a point on the measured surface, and the distance to the surface of the object to be measured is L , which is represented by a blue laser line. A and B are the scan area sizes. During the scanning operation, the shape of the area composed of laser lines changes, as shown in the red laser line in Figure 4. The coordinate system of the optical tracker is O_A . Through the reflective marker point-tracking technology, the coordinate position of the reflective target on the laser three-dimensional scanning probe was obtained at a speed of 60 Hz per second. The phase measurement method was used to calculate the three-dimensional coordinate value ${}^{B_j}P_i$ of each reflective target in the working space of the optical tracker, and the pose matrix ${}^{B_j}P_i$ of the three-dimensional scanner was obtained. If ${}^C P_i$ is a point on a workpiece in the

O_B coordinate system, the three-dimensional coordinates of the laser line projection point in the binocular camera coordinate system O_C are ${}^B P_i$, the three-dimensional coordinates in the optical tracker coordinate system O_A are ${}^A P_i$:

$${}^A P_i = {}^B T_A {}^C T_B {}^C P_i \tag{1}$$

where ${}^C T_B$ is the conversion matrix between the coordinate system O_B and the binocular camera coordinate system O_C of the 3D scanning probe; ${}^B T_A$ is the conversion matrix between the coordinate system O_A of the optical tracker and the coordinate system O_B of the 3D dimensional scanning probe. It is obtained from the attitude matrix $[{}^B P_i]$ of tracking target coordinates.

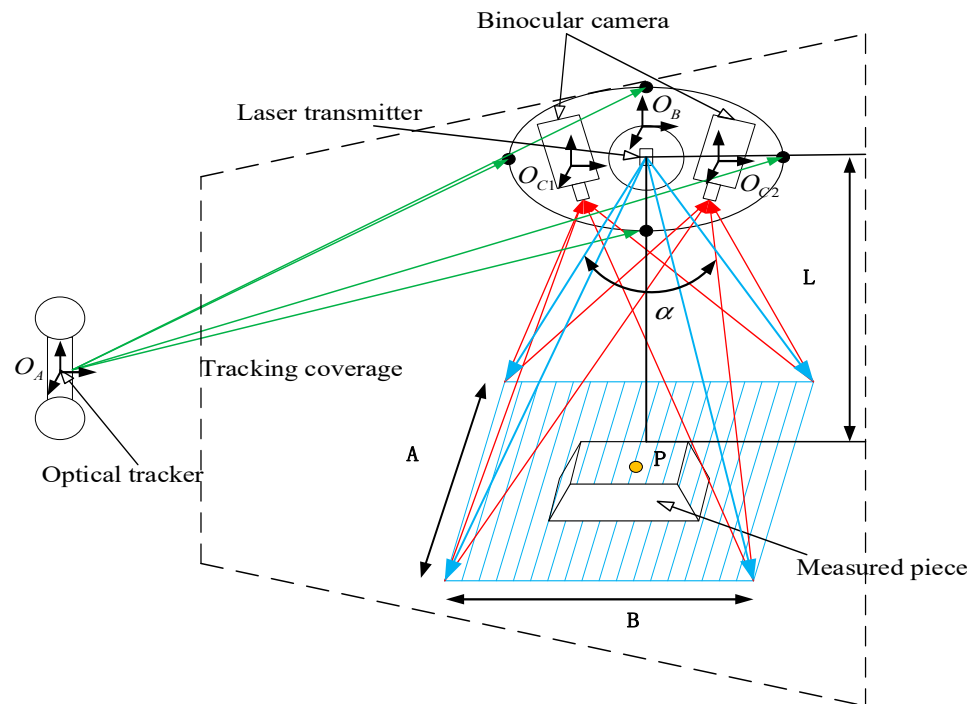


Figure 4. Scanner point cloud scanning principle.

Using the linear three-dimensional information obtained by the three-dimensional scanner and the relative position of the optical tracker in space, when the scanner moves, the three-dimensional information of the position where the laser passes is continuously obtained, thereby forming continuous three-dimensional point cloud data. The free surface data or geometric data of the measured object will be obtained from each image and calculated by the software. The 3D laser scanner model in this paper is Metra SCAN 3D, and its specific parameters are shown in Table 1. The working distance between the scanner and the workpiece surface is 20–40 cm. When the optimal reference distance is 30 cm, the scanning field of the 3D scanner is 27.5 cm × 25 cm, as shown in Figure 5. Due to the use of active shutter technology, it has good adaptability to the surface of workpieces with different degrees of grayness, and can collect enough pictures to achieve efficient scanning.

Table 1. Metra SCAN 3D scanner parameters.

| Accuracy (mm) | Resolution Ratio (mm) | Base Distance L (mm) | Scan Area A × B (mm) | Measuring Rate (r/s) |
|---------------|-----------------------|----------------------|----------------------|----------------------|
| 0.03 | 0.05 | 300 | 275 × 250 | 480,000 |

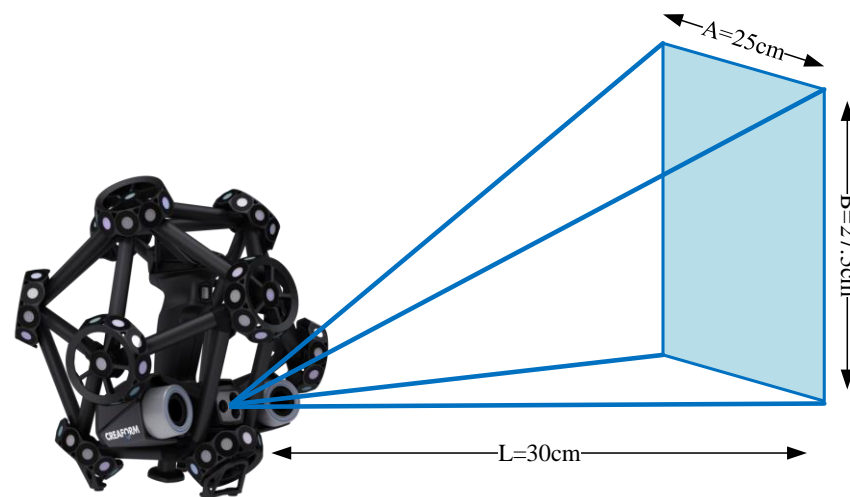


Figure 5. Metra SCAN 3D scanning acquisition area.

3. Scan Path Planning

3.1. Casing Characteristics and Scanning Path Analysis

In the automatic tracking 3D scanning measurement system, the 3D scanning probe is used as the effector of the robot. The robot controls the scanner and moves in the measurement area of the optical tracker for scanning measurement. The scanner needs to move along a straight line and adjust its posture during the scanning process. Therefore, the critical factors in determining the scanning efficiency were the total length of the scanning path and the number of scanner attitude adjustments. In this paper, the scanning object is the aeroengine casing. The overall shape is a thin-walled conical barrel, and the surface has a multi-stiffener structure. The radial diameter random-casing shell changes in height, as shown in Figure 6. According to the geometric characteristics and wall-thickness measurement requirements of the part, to achieve high-efficiency and high-quality scanning reconstruction, a circular scanning path-planning method [20,21] was proposed.

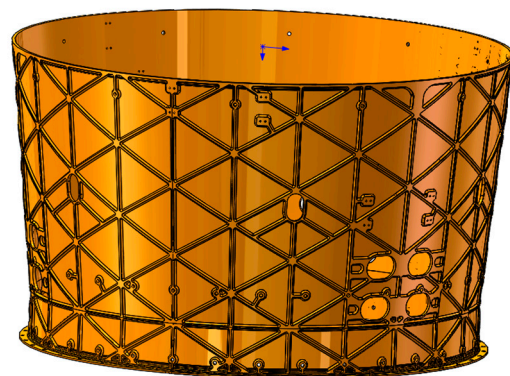


Figure 6. Aero engine casing part.

3.2. Mathematical Modeling of the Circular Scan Path

To facilitate the 3D scanner to scan the inside and outside of the casing, the casing was fixed on the six degrees of freedom parallel tooling support platform in the direction of the radius. In order to avoid the interference collision between the 3D scanner and the six degrees of freedom support platform, bottom-up layer-by-layer circular scanning was adopted. The whole scanning process was divided into two parts: one part is a circular rotating scan around the inner and outer walls of the magazine, and the other part is a straight translation scan along the outer wall of the engine magazine. In the first part of the circular scanning process, the scanner performs a linear translation motion along the

circumcircle tangent of the engine casing. When the scanner moved beyond the acquisition distance, the attitude of the scanner was adjusted. That is, the equidistant offset rotation scanning trajectory was fitted by a multi-segment linear translation motion. Therefore, the total length of the scanner’s linear movement and the number of pose adjustment times were important indicators to evaluate the efficiency of the scanning path-planning strategy.

The scanning starting point of the scanner was set as point A, and the movement mode of the robot within the effective measurement range of the scanner was linear translation. AW is the optimal measurement distance of 30 cm, θ is the angle of the longitudinal direction of the scanning sector, where $\theta = 50^\circ$, A_iB_i, A_iC_i is the distance from the laser line to the surface of the workpiece, where $A_iB_i, A_iC_i \in [20 \text{ cm}, 40 \text{ cm}]$, H is the height of the casing, R_0 is the radius of the casing bottom and β is the cone of the casing. When the robot reaches the maximum capacity of the scanning sector near point A_1 , it completes a linear translation. When the scanner moves to A_1 , the scanning area changes, and the intersection points of the vertex, the boundary and the center O currently are, respectively, represented by red dotted lines in Figure 7a. Scanning along points A, A_1, A_2, \dots, A_n , and completing the first scan, the scanning trajectory is an external polygon, as shown in Figure 7a. The scanner moves points A, E, and F, upward along the outer wall of the casing, and completes the scanning of the A–F ring until the scanning was completed.

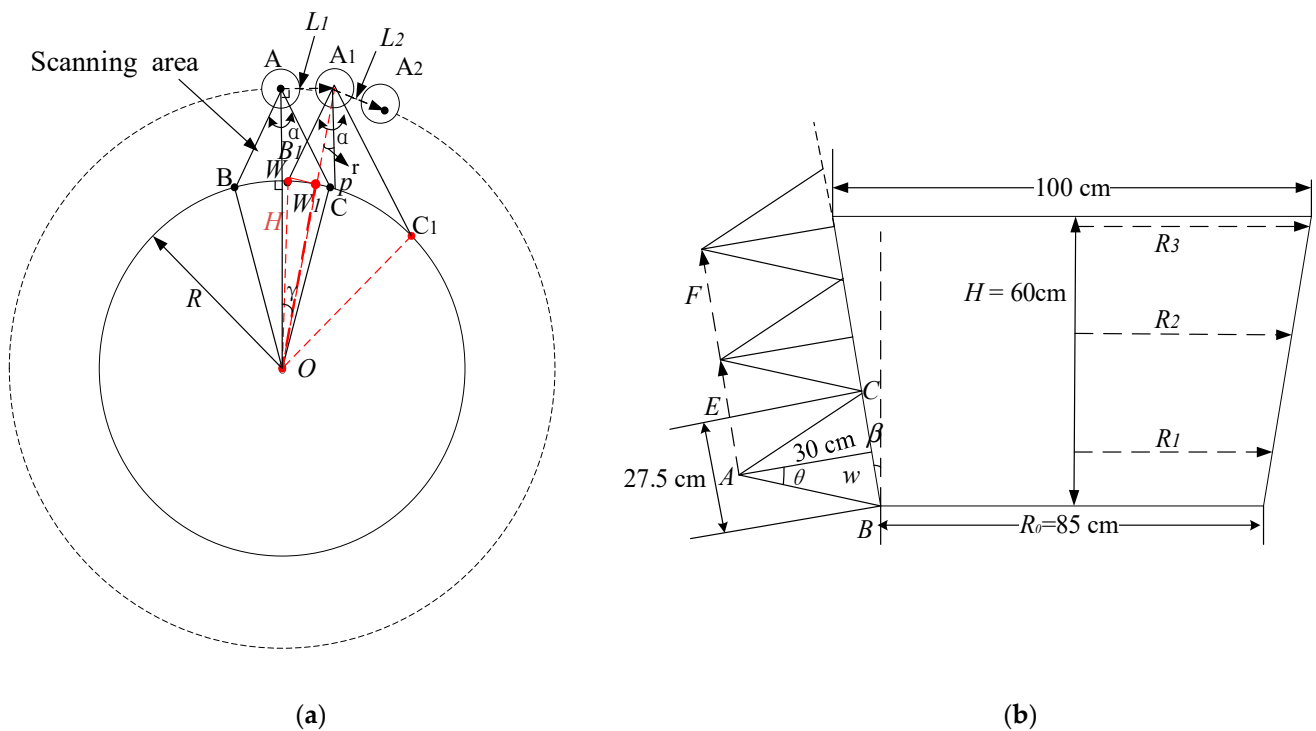


Figure 7. Circular scanning trajectory diagram. (a) Circular scanning top view; (b) Circular scanning main view.

The Establishment of the Mathematical Model of Circular Scanning

1. Circular scanning process

It is assumed that the starting point of the scanner is A and OA is the distance from the scanning area to the center of the casing. The translational scanning motion reaches the pose adjustment point A_1 , OA_1 is the distance from the scanning area to the center of the casing and then there is $OA_i = R_i + AW$. The deflection angle between OA and OA_1 was γ , and the distance between point A and point A_1 was L_1 . According to the geometric position relationship of the three, the length of the scanning trajectory in the measurement range of the scanner is as follows:

$$L = n \sum_{i=1}^m \tan \gamma (R_i + AW) \tag{2}$$

where i is the number of circles scanning; R_i is the scanning radius of circles scanning.

According to the height H_i of the casing and the cone angle β of the casing, the corresponding radius equation of the scanning is as follows:

$$R_i = (2i - 1) \frac{27.5}{2} \sin \beta + R_0 \tag{3}$$

The number of times the scanner adjusts the pose n is as follows:

$$n = \frac{360^\circ}{\gamma} \tag{4}$$

In Figure 7, after the scanner reaches the pose adjustment point A_1 , there are regional boundaries A_1B_1 and A_1C_1 with the geometric position generated on the outer surface of the casing. AW is the angular bisector of angular $\angle BAC$, and the following relationship was obtained:

$$\begin{cases} \cos(\frac{\alpha}{2} - \gamma) = \frac{A_iB_i^2 + OA_i^2 - R_i^2}{2A_iB_iOA_i} \\ \cos(\frac{\alpha}{2} + \gamma) = \frac{A_iC_i^2 + OA_i^2 - R_i^2}{2A_iC_iOA_i} \\ OA_i = \frac{(R_i + AW)}{\cos \gamma} \end{cases} \tag{5}$$

Equation (5) above can obtain the calculation formula of the deflection angle γ :

$$\begin{cases} \gamma = \arccos \left[\frac{(R + A_1W_1)^2 + AC^2 - R^2}{2(R + A_1W_1)AC} \right] - \frac{\alpha}{2} \\ \gamma = \frac{\alpha}{2} - \arccos \left[\frac{(R + A_1W_1)^2 + AB^2 - R^2}{2(R + A_1W_1)AB} \right] \end{cases} \tag{6}$$

where $\cos \frac{\alpha}{2} = \frac{AB^2 + OA^2 - R_1^2}{2AB \times OA}$.

2. Judgment of the scanning boundary

The scanning field of view corresponding to the laser beam of the scanner is shown in Figure 8. When the initial position of the scanner is at point A, the scanning field width angles in both directions are individually $\alpha = 45^\circ$ and $\theta = 50^\circ$. When the AW is 30 cm, the effective field width of the transverse scanning is 25 cm and the effective field width of the vertical scanning is 27.5 cm.

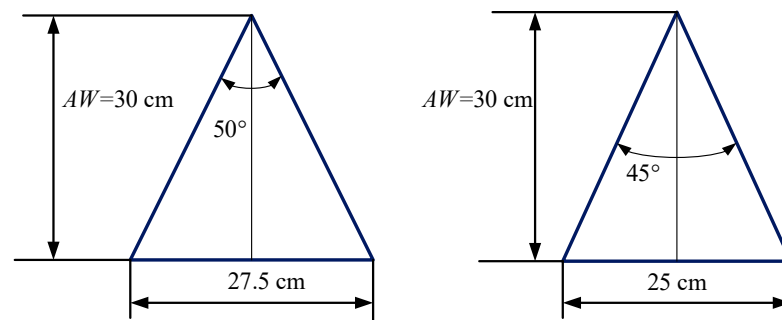


Figure 8. The horizontal and vertical field of view of the scanning area of the scanner.

According to the standard geometric position relationship between the scanner and the cartridge in Figure 7, when the deflection angle $\gamma = 0^\circ$, the boundary distance to the enclosure when the standard position was obtained according to Equation (6):

$$AB = AC = (R + AW)\cos\frac{\alpha}{2} - \sqrt{(R + AW)^2(\cos\frac{\alpha}{2})^2 - (R + AW)^2 + R^2} \quad (7)$$

3. The boundary judgment of the translation limit

When the scanner moves along the casing arc offset tangent, the laser beams AB and AC on both sides of the scanning area also move. The intersection point of the A_1B_1 laser beam irradiated on the casing arc is point B_1 . When A_1B_1 coincides with the intersection point W of the standard position angle branch to the arc, the length of A_1B_{1min} is the smallest, which is the boundary of the reference scanning area:

$$A_1B_{1min} = \sqrt{AW^2 + (\frac{25}{2})^2} = 32.5 \text{ cm} \quad (8)$$

According to Equations (7) and (8), when AW is in the effective area of the deflection angle, A_1B_1 conforms to the boundary constraint condition in the translation process. Then, judge A_1C_1 , let $A_1C_{1max} = 40$ cm. According to Equation (6), the limit boundary judgment equation of scanning translation is as follows:

$$\begin{cases} A_1C_1 = (R + A_1W_1)\cos(\frac{\alpha}{2} + \gamma) - \sqrt{(R + A_1W_1)^2[\cos(\frac{\alpha}{2} + \gamma)]^2 - (R + A_1W_1)^2 + R^2} \\ A_1B_1 = (R + A_1W_1)\cos(\frac{\alpha}{2} - \gamma) - \sqrt{(R + A_1W_1)^2[\cos(\frac{\alpha}{2} - \gamma)]^2 - (R + A_1W_1)^2 + R^2} \end{cases} \quad (9)$$

The variation range of the deflection angle is obtained by simplifying Equation (9):

$$0 \leq \gamma \leq \arccos\frac{(R + A_1W_1)^2 + AC^2 - R^2}{2(R + A_1W_1)AC} - \frac{\alpha}{2} \quad (10)$$

where $AC \leq 40$ cm; $A_1W_1 = \frac{R+AW}{\cos\gamma} - R$.

4. The rising posture adjustment process

After completing the first ring scan, the scanner returns to the starting point A . The scanner continued to move up along the outer wall of the casing to reach point E , and the distance between the two points is K_1 . Move up m times in a turn, obtain the final point F , and complete m -cycle scanning:

$$m = \frac{H}{\cos\beta \times 27.5} \quad (11)$$

$$K_1 = \frac{H_i - H_{i-1}}{\cos\beta}; i \geq 2 \quad (12)$$

where 27.5 cm is the effective scanning area of the scanner in the vertical direction.

Assuming that the total distance of the robot moving upward is K , according to Equations (11) and (12) above, the mathematical expression of the upward translation parallel to the outer wall of the casing is as follows:

$$K = mk_1 = \frac{H(H_i - H_{i-1})}{27.5(\cos\beta)^2} \quad (13)$$

According to Equations (2) and (13), the mathematical expression of the total distance Q of the circular scanning is as follows:

$$Q = n \sum_{i=1}^m \tan \gamma (R_i + AW) + \frac{H(H_i - H_{i-1})}{27.5(\cos \beta)^2} \tag{14}$$

The total number of posture adjustments of the annular scanning method is n :

$$n = \sum_{i=1}^m \frac{360^\circ}{\gamma_i} \tag{15}$$

3.3. Repeat the Scan Area Compensation Method

Substitute the measured casing height $H = 60$ cm into Equation (11) to obtain the number of scans, not the number of full turns. In the scanning process, the number of scans should also be rounded to achieve complete scanning reconstruction. In this paper, each circle's scanning height was adjusted to decrease the scanning area, and the repeated scanning area was divided into each ring. The corresponding scanning radius R_i will change, and the average coefficient v compensation method was used to compensate for the repeated scanning area. Taking the scanning casing as an example, there are:

$$v = \frac{3 - 2.198}{3} = 0.267 \tag{16}$$

$$H_{iv} = H - H \times v \tag{17}$$

According to Equations (3), (16) and (17), the distance between the scanner and the casing before and after scanning was obtained by adjusting the scanning height, as shown in Table 2.

Table 2. The distance relationship between the scanner and the corresponding position of the casing before and after adjusting the scanning height (unit cm).

| m_i | H_i | R_i | H_{iv} | R_{iv} |
|---------|-------|-------|----------|----------|
| $i = 1$ | 13.64 | 44.21 | 9.99 | 43.75 |
| $i = 2$ | 40.92 | 47.62 | 29.99 | 46.25 |
| $i = 3$ | 68.20 | 51.03 | 49.99 | 48.75 |

According to the data in Table 2, the corresponding position relationship diagram before and after scanning height adjustment is shown in Figure 9. It can be seen from Figure 9 that the adjusted H_{iv} is lower than the corresponding height H of the original scan, and the corresponding R_{iv} of the scan is lower than the original scan radius R as a whole.

Using the above established circular scanning path-planning method, the relevant data of the scanning path before and after the scanning height adjustment were calculated as shown in Tables 3 and 4.

Table 3. The relevant data of the casing scanning path before adjustment (in cm).

| Order Number | Angle of Deflection | The Number of Postures | Surround Path Length | Rising Path Length | Total Path Length |
|--------------|---------------------|------------------------|----------------------|--------------------|-------------------|
| 1 | 5.8° | 63 | 472.5 | 0 | 472.5 |
| 2 | 6.2° | 59 | 487.74 | 27.49 | 487.74 |
| 3 | 6.7° | 54 | 510.447 | 27.49 | 510.447 |
| Total | – | 176 | 1470.687 | 54.98 | 1525.67 |

Table 4. The relevant data of the casing scanning path after adjustment (in cm).

| Order Number | Angle of Deflection | The Number of Postures | Surround Path Length | Rising Path Length | Total Path Length |
|--------------|---------------------|------------------------|----------------------|--------------------|-------------------|
| 1 | 5.5° | 66 | 462 | 0 | 462 |
| 2 | 6° | 60 | 487.2 | 20.15 | 507.35 |
| 3 | 6.5° | 56 | 504 | 20.15 | 5245.1 |
| Total | | 182 | 1453.2 | 40.3 | 1493.5 |

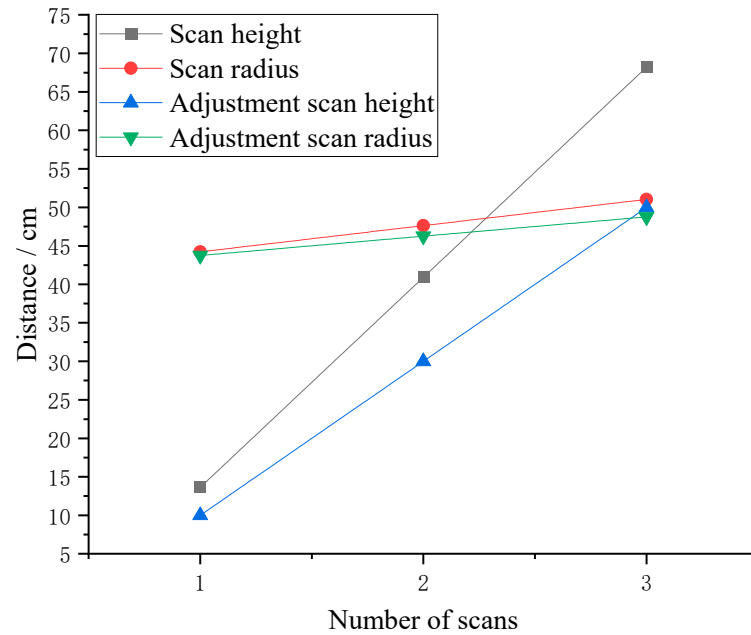


Figure 9. Scanning height adjustment before and after scanning the corresponding position diagram.

If the scanning speed is $v = 0.04$ m/s and the posture adjustment time is $t = 0.5$ s/n, the total time to complete the casing scanning before and after the adjustment is as follows:

$$\begin{cases} T_{\text{before}} = \frac{Q}{v} + Nt = 381.4175 + 88 = 469.417 \text{ s} \\ T_{\text{after}} = \frac{Q}{v} + Nt = 373.375 + 91 = 464.375 \text{ s} \end{cases} \quad (18)$$

Through the analysis of the relevant data of the scanning path before and after the above scanning height adjustment it can be seen that the scanning range distribution can be changed by adjusting the scanning height, the complete scanning of the workpiece can be realized and the scanning quality is better than before the adjustment.

3.4. Analysis of the Scan Path Parameters

The casing geometry is shown in Figure 7, where the casing cone angle β is 7.125° . According to the corresponding data after adjusting the scanning height in Table 4, the ring scanning radius R_1 of the scanner in the first circle is 43.75 cm. In the process of annular scanning in the limited scanning area, the changes in related parameters such as γ , A_1W_1 , A_1B_1 , A_1C_1 and L in the scanning path are shown in Table 5. The relationship between the deflection angle and the scanning distance was plotted, as shown in Figure 10.

Table 5. Relationship Data between Deflection Angle and Scan Distance (first circle) (in cm).

| Number | γ | A_1B_1 | A_1C_1 | A_1W_1 | L |
|--------|----------|----------|----------|----------|------|
| 1 | 0° | 34.70 | 34.70 | 30 | 0 |
| 2 | 1° | 34.23 | 35.25 | 30.01 | 1.29 |
| 3 | 2° | 33.83 | 35.89 | 30.06 | 2.58 |
| 4 | 3° | 33.53 | 36.67 | 30.16 | 3.87 |
| 5 | 4° | 33.36 | 37.64 | 30.34 | 5.18 |
| 6 | 5° | 33.32 | 38.85 | 30.62 | 6.50 |
| 7 | 6° | 33.45 | 40.39 | 31.03 | 7.86 |
| 8 | 7° | 33.76 | 42.37 | 31.59 | 9.25 |

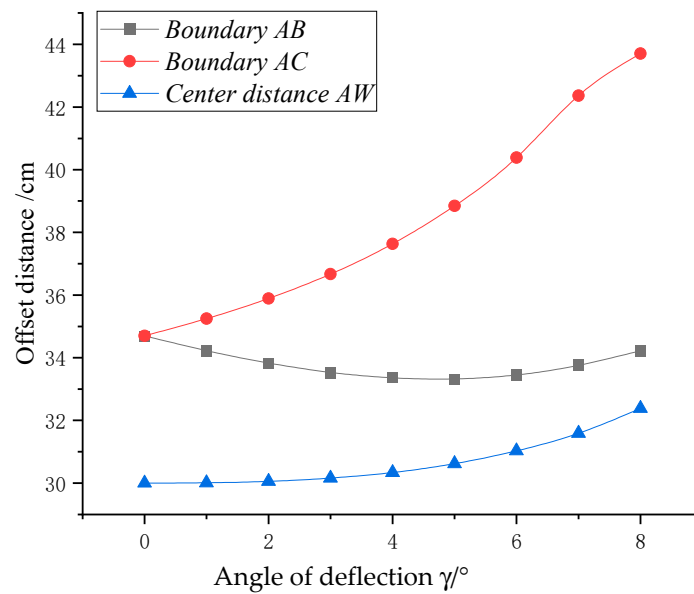


Figure 10. Curve diagram of the relationship between deflection angle and scanning distance.

It can be seen from Table 5 that the deflection angle γ at 0–5° is an effective scanning range in the first circular scanning. When $\gamma = 0^\circ$, the scanner is in the standard position, and the distance between A_1C_1 and A_1B_1 and the scanner is equal. The laser beam at the boundary of the scanner is an isosceles triangle. It can be seen from Figure 10 that A_1W_1 and A_1C_1 increase with the increase in γ . When the deflection angle γ is between 0–4°, A_1B_1 decreases with the increase in γ . When the deflection angle γ is 4–5°, A_1B_1 increases with the increase in γ .

During the second and third rounds of scanning, the radius of the casing gradually increases, and the corresponding scanning radius and deflection angle increase to varying degrees. The data of the relationship between the deflection angle of the second and third turns and the scanning distance are shown in Tables 6 and 7, respectively.

Table 6. Deflection angle and scan distance relationship data (second circle) (in cm).

| Number | γ | A_1B_1 | A_1C_1 | A_1W_1 | L |
|--------|----------|----------|----------|----------|------|
| 1 | 0° | 34.56 | 34.56 | 30 | 0 |
| 2 | 1° | 34.10 | 35.08 | 30.01 | 1.33 |
| 3 | 2° | 33.72 | 35.70 | 30.06 | 2.66 |
| 4 | 3° | 33.45 | 36.45 | 30.16 | 4.01 |
| 5 | 4° | 33.29 | 37.38 | 30.35 | 5.35 |
| 6 | 5° | 33.27 | 38.55 | 30.64 | 6.72 |
| 7 | 6° | 33.42 | 40.04 | 31.06 | 8.12 |
| 8 | 7° | 33.76 | 41.94 | 31.64 | 9.56 |

Table 7. Relationship Data of Deflection Angle and Scan Distance (third circle) (in cm).

| Number | γ | A_1B_1 | A_1C_1 | A_1W_1 | L |
|--------|----------|----------|----------|----------|-------|
| 1 | 0° | 34.43 | 34.43 | 30 | 0 |
| 2 | 1° | 33.99 | 34.94 | 30.01 | 1.37 |
| 3 | 2° | 33.63 | 35.53 | 30.05 | 2.75 |
| 4 | 3° | 33.37 | 36.26 | 30.16 | 4.13 |
| 5 | 4° | 33.23 | 37.17 | 30.36 | 5.531 |
| 6 | 5° | 33.23 | 38.30 | 30.66 | 6.94 |
| 7 | 6° | 33.41 | 39.75 | 31.09 | 8.38 |
| 8 | 7° | 33.77 | 41.59 | 31.69 | 9.87 |

Figure 11 shows the relationship between the deflection angle, scanning radius and scanning distance in the second circular scanning. It can be seen from Figure 11 that when the scanner rises for scanning, the deflection angle γ increases with the increase in the corresponding scanning radius and the corresponding scanning path also increases.

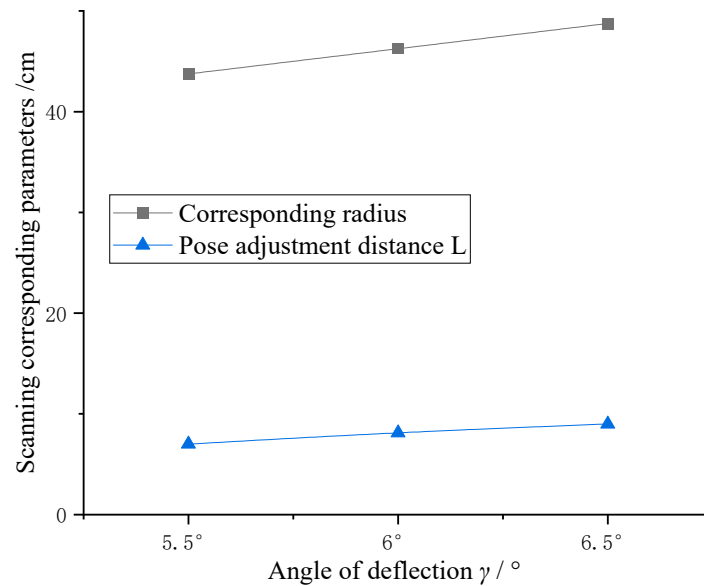


Figure 11. Deflection angle and scan corresponding parameters.

4. Scanning Simulation Analysis

4.1. Description of the Scan Trajectory Motion

In the circular scanning motion, the scanning motion is regarded as the motion of the robot tool coordinate system $\{T\}$ relative to the workpiece coordinate system $\{S\}$, both translational motion and rotational motion. As shown in Figure 12, the workpiece coordinate system $\{S\}$ is used as the reference coordinate system, and the starting point is set to P_0 . Due to the limited scanning range of the scanner, it is necessary to adjust the attitude when reaching the coordinate point P_1 . The scanning trajectory of the first circle passes through the coordinate point P_i, P_{i+1}, \dots, P_n in turn. The rising part of the trajectory passes through the coordinate P_j, P_{j+1} , the scanner will only have a translational motion until the scan was complete. The spatial pose of the scanner's scanning trajectory coordinates is expressed as:

$$\begin{aligned}
 {}^S P_0 &= {}^T P_0 + {}^T P_{S0}; \quad {}^S P_1 = {}^0 T^S P_0; \quad {}^S P_2 = {}^0 T_2^1 T^S P_0; \quad {}^S P_3 = {}^0 T_2^1 T_3^2 T^S P_0; \\
 {}^S P_i &= {}^0 T_2^1 T_3^2 T_i^{i-1} T^S P_0; \quad {}^S P_{i+1} = {}^0 T_2^1 T_3^2 T_i^{i-1} T_{i+1}^i T^S P_0; \\
 {}^S P_n &= {}^0 T_2^1 T_3^2 T_i^{i-1} T_{i+1}^i T_n^{n-1} T^S P_0 = {}^n T^S P_0 \\
 {}^S P_m &= {}^m T P_0
 \end{aligned} \tag{19}$$

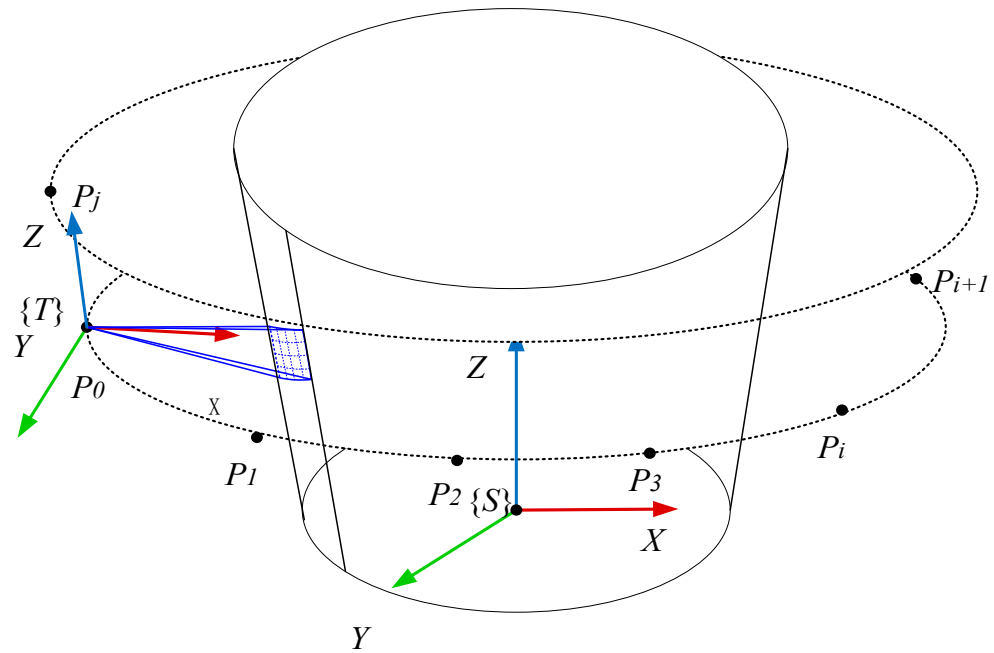


Figure 12. Schematic diagram of the circular scan trajectory.

The coordinate expression of any coordinate point in the scanning trajectory is as follows:

$${}^sP_{nm} = ({}^0_nT^s + {}^0_mT)P_0 \tag{20}$$

$$\text{where } {}^0_nT = \text{rot}(z, \sum_{i=0}^n \gamma_i) \text{trans}(\sum_{i=0}^n l_i) = \begin{bmatrix} \cos \sum_{i=0}^n \gamma_i & -\sin \sum_{i=0}^n \gamma_i & 0 & 0 \\ \sin \sum_{i=0}^n \gamma_i & \cos \sum_{i=0}^n \gamma_i & 0 & \sum_{i=0}^n l_i \\ 0 & 0 & 1 & 0 \\ 0 & 0 & 0 & 1 \end{bmatrix}; {}^i_mT = \text{trans}Z(\sum_{j=2}^m k_j) = \begin{bmatrix} 0 \\ 0 \\ K_j \\ 1 \end{bmatrix}.$$

The curve circle model is created with $(R + AW)$ as the radius. The coordinate $P_0 = [R_i + AW, l_i, H_i]^T$ of the starting point of the scanning path is set. Based on Equation (20), the coordinate position of the coordinate point P_i on the scanning trajectory was solved, and the scanning trajectory was fitted.

4.2. Establishment of Scanning Simulation Model

To verify the rationality of the above scanning path planning, the robot studio robot simulation software is used to simulate the virtual scanning trajectory motion under the condition of 3D scanner parameter constraints. The ABB-IRB6700 model robot and the casing part model were imported into the software, and the robot system was created by the 'layout' method. Select the frame creation method to establish the tool and workpiece coordinate system, generate the scanner tool and install it on the robot end effector. Adjust the position and angle of the imported model to make it in the robot workspace.

In the workpiece coordinate system, the scanning motion parameters were set, the running speed is $v = 0.04$ m/s, the acceleration is $a = 0.5$ m/s and the posture adjustment time is $t = 0.5$ s. The obtained scanning trajectory coordinate points were used to set the robot's motion trajectory, generate the robot's motion path and complete the robot's motion trajectory offline programming. Run the scanning trajectory program to perform automatic scanning trajectory simulation motion, and the scanning motion process is shown in Figure 13.

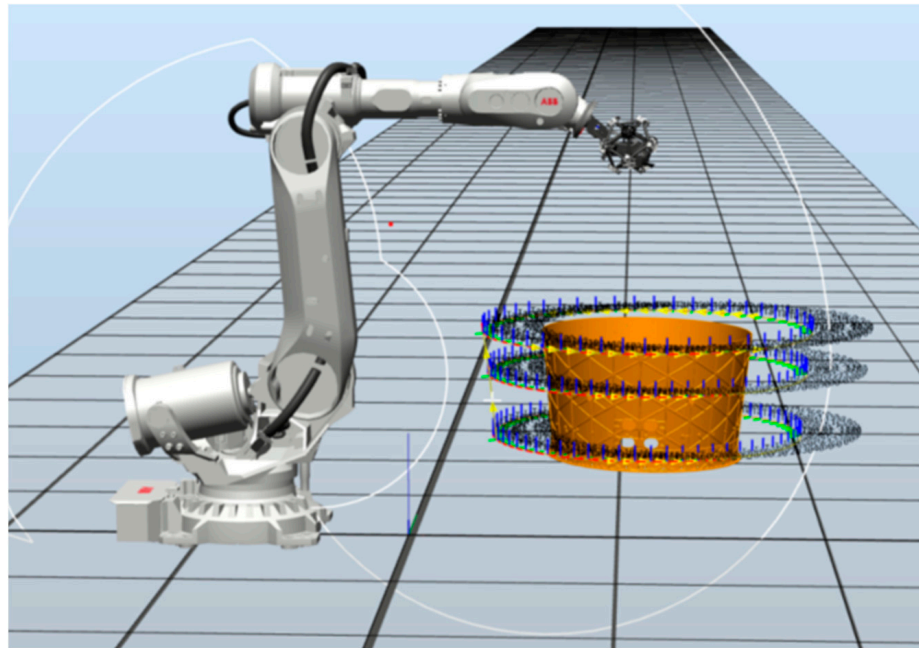


Figure 13. Scanning simulation motion. In the figure, the blue line, the red line and the green line are the x , y , z axes of the trajectory point coordinate system, and the yellow arrow is the trajectory motion direction.

In the process of simulation scanning motion, the robot and the 3D scanner did not interfere or collide with the casing. The scanning range conforms to the scanning space constraint condition of the scanner, and the running time is close to the theoretical analysis running time. The off-line scanning trajectory programming based on the geometric characteristics of the measured parts was realized, and the feasibility and correctness of the scanning path planning were also proved.

5. Scanning Measurement Process Experiment

The scanning trajectory of this experiment adopts the scanning trajectory program generated by off-line programming of simulation software, which was imported into the automatic measurement system by downloading and the scanning speed is 0.04 m/s. According to the geometric characteristics and measurement requirements of the casing, the scanning parameter template and the thickness measurement template were established, respectively, to realize the automatic scanning reconstruction and automatic measurement of the casing. The scanning process is shown in Figure 14.

The experimental results show that the whole ring scanning time is about 15 min, including robot start-up and return movement. The casing scanning reconstruction model has a complete quality and no obvious noise. For the measurement of the casing parts, the total time of scanning and measurement using this system was 60 min, including scanning path programming, measurement template preparation, scanning and post-processing. However, manual measurement using an ultrasonic thickness gauge requires two hours for six people to measure at the same time and the scanning efficiency is increased by more than 80%. The least squares algorithm was used to fit the obtained point cloud data and the model was reconstructed after the workpiece was scanned, as shown in Figure 15.

By establishing the thickness measurement template, the thickness measurement was completed for the engine magazine works. The thickness deviation between the scanned model and the design model is shown more intuitively in the form of a chromatogram to evaluate the quality of the casing milling, as shown in Figures 16 and 17. Comparing the measured values of the three-dimensional scanning in the same area with the measured values measured by the ultrasonic thickness gauge, the deviation of the measured values is

within 0.1–0.2%. This error is likely to be caused by the deviation of the measurement position. The measurement accuracy of the measurement method can meet the measurement of such workpieces.

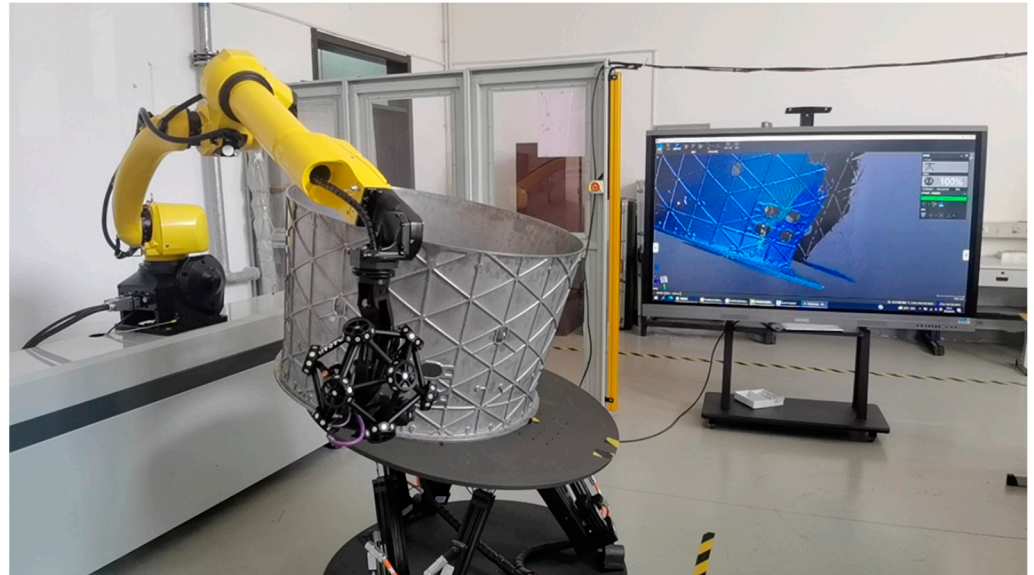


Figure 14. Casing scanning process.

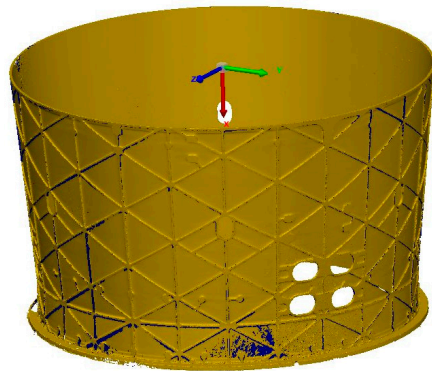


Figure 15. After the scanned artifact reconstruction model.

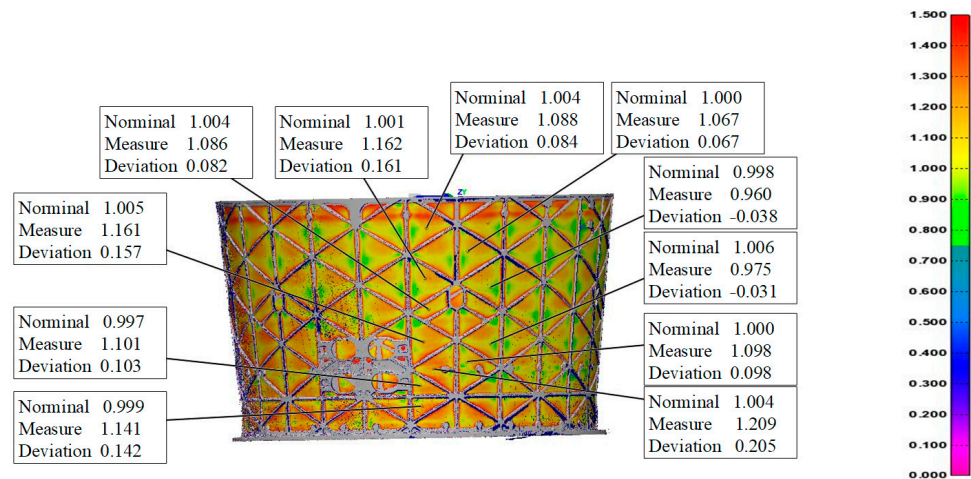


Figure 16. Casing surface thickness chromatogram.

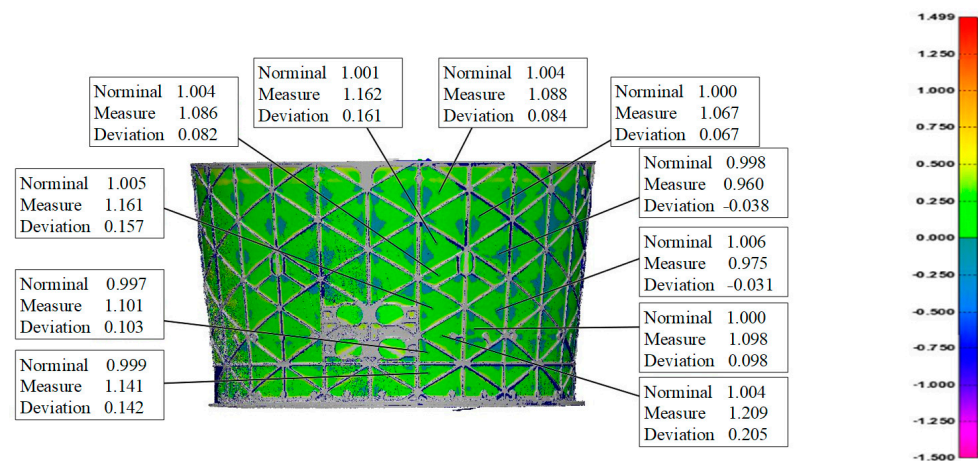


Figure 17. Casing surface thickness deviation chromatogram.

6. Conclusions

In this paper, a non-contact automatic three-dimensional scanning measurement process system and process are proposed and established for the rapid and high-precision measurement requirements of aero-engine casing parts. The scanning trajectory is analyzed and verified by mathematical modeling, simulation analysis and process test. The main conclusions are as follows:

- (1) According to the relationship between the scanning area constraint of the scanner and the geometric size of the casing, a mathematical model of the annular scanning trajectory is established. The scanning path planning from part model to off-line robot programming was realized. The scanning path-planning method is suitable for the scanning measurement of cylindrical parts with tapering, such as casing parts;
- (2) It is proposed to evenly distribute the scanning repetition area by adjusting the scanning height, and introducing the square compensation coefficient to compensate for the repeated scanning area. Through the numerical calculation of the scanning path before and after the adjustment, it is found that the allocation method shortens the scanning path by 1.1%, and the scanning integrity is also improved;
- (3) The robot-studio software is used to conduct the motion simulation of the optimized scanning path and verify the scanning process experiment. The results show that the annular trajectory scanning method established in this paper can meet the scanning measurement requirements of casing parts. The efficiency of scanning measurement is more than 80% higher than that of artificial ultrasonic point-by-point measurement.

Author Contributions: Conceptualization, J.L. and M.W.; methodology, L.Q.; formal analysis, G.L.; investigation, J.L.; data curation, J.L.; writing—original draft preparation, J.L.; writing—review and editing, M.W.; supervision, L.Q.; project administration, G.L.; funding acquisition, J.L. All authors have read and agreed to the published version of the manuscript.

Funding: This research was funded by the Liaoning Province ‘Xingliao Talent Plan’ project, grant number XLYC2002086; the Discipline Construction Fund, grant number 310121001 and the National Key Research and Development Plan by Liaoning, grant number 2022JH2/101300211.

Institutional Review Board Statement: Not applicable.

Informed Consent Statement: Not applicable.

Data Availability Statement: Not applicable.

Conflicts of Interest: The authors declare no conflict of interest.

References

1. Srinivas, G.; Kurkal, R.; Shenoy, S.B. Recent developments in turbomachinery component materials and manufacturing challenges for aero engine applications. *IOP Conf. Ser. Mater. Sci. Eng.* **2018**, *314*, 012012. [[CrossRef](#)]

2. Xu, F.; Yang, M.; Chai, X.; Yan, K.; Ni, X. Lightweight design method of aero-engine combustor case. *Aeronaut. Sci. Technol.* **2021**, *32*, 27–34. [[CrossRef](#)]
3. Liu, L.; Wang, E.; Zhang, X.; Liang, W.; Li, X.; Xie, H. MEMS-based 3D confocal scanning microendoscope using MEMS scanners for both lateral and axial scan. *Sens. Actuators A Phys.* **2014**, *215*, 89–95. [[CrossRef](#)] [[PubMed](#)]
4. Popov, I.; Onuh, S.; Dotchev, K. Dimensional error analysis in point cloud-based inspection using a non-contact method for data acquisition. *Meas. Sci. Technol.* **2010**, *21*, 075303. [[CrossRef](#)]
5. Gerde, J.R.; Christens-Barry, W.A. Evaluating a hybrid 3-dimensional metrology system: Merging data from optical and touch probe devices. In Proceedings of the SPIE Optical Engineering+ Applications 2011, San Diego, CA, USA, 21–25 August 2011. [[CrossRef](#)]
6. Chu, C.L.; Wu, C.Y. Development of 3D touch trigger probe with real-time observation. In Proceedings of the 6th International Symposium on Precision Engineering Measurements and Instrumentation, Hangzhou, China, 8–10 August 2010. [[CrossRef](#)]
7. Elkott, D.; Veldhuis, S. CAD-based sampling for CMM inspection of models with sculptured features. *Eng. Comput.* **2007**, *23*, 187–206. [[CrossRef](#)]
8. Hot, J.; Dasquec, A.; Topalov, J.; Mazars, V.; Ringot, E. Titanium valorization: From chemical milling baths to air depollution applications. *J. Clean. Prod.* **2020**, *249*, 119–344. [[CrossRef](#)]
9. Phan, N.D.M.; Quinsat, Y.; Lavernhe, S.; Lartigue, C. Scanner path planning with the control of overlap for part inspection with an industrial robot. *Int. J. Adv. Manuf. Technol.* **2018**, *98*, 629–643. [[CrossRef](#)]
10. Mahamood, R.M.; Akinlabi, E.T. Chemical Cutting Process. In *Advanced Noncontact Cutting and Joining Technologies*; Springer: Berlin/Heidelberg, Germany, 2018; pp. 11–25. [[CrossRef](#)]
11. Zhang, C.; Zhao, H.; Qiao, J.; Zhou, C.; Zhang, L.; Hu, G.; Geng, H. Three-dimensional measurement based on optimized circular fringe projection technique. *Opt. Express* **2019**, *27*, 2465–2477. [[CrossRef](#)] [[PubMed](#)]
12. Elkott, D.F.; Veldhuis, S.C. Isoperimetric line sampling for the inspection planning of sculptured surfaces. *Comput.-Aided Des.* **2004**, *37*, 189–200. [[CrossRef](#)]
13. Duan, X.; Wang, C.; Wang, J.; Zhao, H. A new calibration method and optimization of structure parameters under the non-ideal condition for 3D measurement system based on fiber-optic interference fringe projection. *Opt. Int. J. Light Electron.* **2018**, *172*, 424–430. [[CrossRef](#)]
14. Wang, Y.D. The Applications of Industrial Robots in the Field of Industrial Automation and Control. *Int. Conf. Front. Manuf. Sci. Meas. Technol.* **2013**, *401–403*, 1716–1719. [[CrossRef](#)]
15. Li, D.; Tian, J.; Yang, X. A new 3D measurement method and its calibration based on the combination of binocular and monocular vision. *Proc. SPIE-Int. Soc. Opt. Eng.* **2012**, *8563*, 9. [[CrossRef](#)]
16. Boulch, A.; Guerry, J.; Le Saux, B.; Audebert, N. 3D point cloud semantic labeling with 2D deep segmentation networks. *Comput. Graph.* **2018**, *71*, 189–198. [[CrossRef](#)]
17. Yang, Y.; Li, Z.; Yu, X.; Li, Z.; Gao, H. A trajectory planning method for robot scanning system using mask R-CNN for scanning objects with unknown model. *Neurocomputing* **2020**, *404*, 329–339. [[CrossRef](#)]
18. Njaastad, E.B.; Munthe-Kaas, N.H.; Egeland, O. Robotic Autoscanning of Highly Skewed Ship Propeller Blades. *IFAC-Pap. On-Line* **2018**, *51*, 435–440. [[CrossRef](#)]
19. Song, C.K.; Kim, S.W. Reverse engineering: Autonomous digitization of free-formed surfaces on a CNC coordinate measuring machine. *Int. J. Mach. Tools Manuf.* **1997**, *37*, 1041–1051. [[CrossRef](#)]
20. Fan, K.C.; Cheng, F.; Wang, W.; Chen, Y.; Lin, J.Y. A scanning contact probe for a micro-coordinate measuring machine (CMM). *Meas. Sci. Technol.* **2010**, *21*, 054002. [[CrossRef](#)]
21. Saadat, M.; Cretin, L. Measurement systems for large aerospace components. *Sens. Rev.* **2002**, *22*, 199–206. [[CrossRef](#)]

Disclaimer/Publisher’s Note: The statements, opinions and data contained in all publications are solely those of the individual author(s) and contributor(s) and not of MDPI and/or the editor(s). MDPI and/or the editor(s) disclaim responsibility for any injury to people or property resulting from any ideas, methods, instructions or products referred to in the content.